Eur. Phys. J. D **7**, 261–267 (1999)

THE EUROPEAN PHYSICAL JOURNAL D

EDP Sciences

Sisyphus cooling of rubidium atoms on the D_2 ($F = 1 \rightarrow F' = 1$) line: The role of the neighbouring transitions

D. Lucas[a], P. Horak[b], and G. Grynberg

Laboratoire Kastler-Brossel, Département de Physique de l'École Normale Supérieure, 24 rue Lhomond, 75231 Paris Cedex 05, France

Received 26 November 1998 and Received in final form 20 April 1999

Abstract. We study one-dimensional Sisyphus cooling on the $5S_{1/2}(F = 1) \rightarrow 5P_{3/2}(F' = 1)$ transition of ^{87}Rb atoms in the electric field created by two counter-propagating linearly polarized laser beams with an angle of θ between the polarization directions. The neighbouring $F' = 0$ and $F' = 2$ excited states are found to play an important role in the cooling mechanism, *e.g.*, by inhibiting a significant population of the velocity-selective dark state. Our experimental data, such as temperatures and probe absorption coefficients, agree well with the results of quantum Monte-Carlo wavefunction simulations.

PACS. 32.80.Pj Optical cooling of atoms; trapping – 32.80.Lg Mechanical effects of light on atoms, molecules, and ions – 32.80.Qk Coherent control of atomic interactions with photons

1 Introduction

The discoveries of polarization gradient cooling [1,2] and velocity-selective coherent population trapping [3] were two major steps in the history of laser cooling. Using the combined effects of optical pumping and light shifts, polarization gradient cooling mechanisms and in particular the Sisyphus effect allow temperatures as low as a few recoil energies [4] to be achieved. However, the recoil energy is an intrinsic border that cannot be crossed without the help of another physical process.

By contrast, velocity-selective coherent population trapping (VSCPT) can be used to reach much lower temperatures [5]. This method suffers however from two severe drawbacks:

(i) the cooling process is relatively slow because it relies on a random walk of atoms in momentum space,
(ii) it generally requires a transition connecting two levels of angular momentum $F = 1$.

In fact, point (i) can be partly circumvented by combining Sisyphus cooling and VSCPT [6–9]. In this case one achieves a fast Sisyphus cooling down to a temperature of a few recoils and a slow VSCPT cooling to lower temperatures afterwards. Point (ii) on the contrary is inherent to the VSCPT method. The most successful experiments [3,5] were done on a transition connecting the metastable 2^3S_1 and the excited 3^3P_1 states of helium. This is a rather difficult experiment which cannot be performed in a cell. There are other atoms and in particular alkalies where a $F = 1 \rightarrow F' = 1$ transition does exist, but apart from one successful experiment on the D_1 line of rubidium [10] there is, to our knowledge, no other experimental evidence of subrecoil temperatures obtained by VSCPT.

In previous experiments, isolated atomic transitions were deliberately chosen. In this work, however, we wished to investigate in detail the influence of neighbouring transitions on dark state cooling, and we study laser cooling of ^{87}Rb atoms near the $5S_{1/2}(F = 1) \rightarrow 5P_{3/2}(F' = 1)$ transition (D_2 line). For the sake of simplicity and to be able to make quantitative comparisons with theory, we limited our study to the case of one-dimensional (1D) cooling. Basically, we used the so-called "lin θ lin" configuration [11] where the two counterpropagating beams have linear polarizations with an angle θ between them.

Our main observation, confirmed by quantum Monte-Carlo wavefunction simulations, is that it is not possible to achieve temperatures below the recoil energy on this system. This is due to the harmful effect of the other hyperfine sublevels of the excited state. Although the laser detuning from the $F = 1 \rightarrow F' = 1$ transition is typically one order of magnitude smaller than that from the $F = 1 \rightarrow F' = 0$ or $F = 1 \rightarrow F' = 2$ transitions, these latter transitions inhibit the dark state cooling.

We have studied the dependence of the temperature on the intensity, detuning and angle θ and find results in excellent agreement with the theoretical predictions. We also performed some experiments with a probe beam and in particular considered how the absorption varies

[a] *Present address*: Clarendon Laboratory, Parks Road, Oxford OX1 3PU, UK.
e-mail: d.lucas@physics.ox.ac.uk
[b] *Present address*: Department of Physics and Applied Physics, University of Strathclyde, Glasgow G4 ONG, UK.

with the probe polarization. Such experiments give some information about the atomic localization. As expected from the temperature measurements, we find a localization which differs from that of the dark state but which is in good agreement with the theoretical prediction.

2 Sisyphus cooling on a dark or nearly dark transition

In this paper we will discuss the cooling of ^{87}Rb atoms in the electric field of two counter-propagating laser beams of linear polarization with an angle θ between the two polarization directions ("lin θ lin" configuration). The two beams have the same amplitude $\mathcal{E}$ and frequency $\omega = ck$ and propagate along Oz. The lasers are tuned close to resonance with the atomic $F = 1 \rightarrow F' = 1$ transition (resonance frequency ω_0). For this laser configuration the spatial dependence of the circularly polarized components of the total electric field is given by

$$a_{\pm}(z) = \mathcal{E}\sqrt{2}\cos(kz \pm \theta/2). \tag{1}$$

2.1 Pure atomic 1 ⟶ 1 transition

The case of a pure $F = 1 \rightarrow F' = 1$ transition, *i.e.*, where all other atomic transitions are sufficiently far detuned that they can be neglected, has already been studied in detail [7], and we will only repeat the basic properties here.

For weak atomic excitation the two adiabatic potentials obtained by diagonalizing the coupling between the two ground states $|m_F = \pm 1\rangle$ are given by

$$V_{\mathrm{NC}}(z) = 0, \tag{2}$$

$$V_{\mathrm{C}}(z) = U_0\left[\cos^2(kz + \theta/2) + \cos^2(kz - \theta/2)\right], \tag{3}$$

where U_0 is the light shift for a single laser beam. Thus, for blue detuning ($\omega > \omega_0$) the lower adiabatic potential is flat, whereas the upper one is spatially modulated for $\theta \neq \pi/2$. The corresponding eigenstates are

$$|\psi_{\mathrm{NC}}\rangle = \frac{1}{\sqrt{D(z)}}\big[\cos(kz - \theta/2)|m_F = -1\rangle + \cos(kz + \theta/2)|m_F = 1\rangle\big], \tag{4}$$

$$|\psi_{\mathrm{C}}\rangle = \frac{1}{\sqrt{D(z)}}\big[-\cos(kz - \theta/2)|m_F = -1\rangle + \cos(kz + \theta/2)|m_F = 1\rangle\big], \tag{5}$$

where $D(z) = 1 + \cos\theta\cos(2kz)$.

The cooling of the atoms in this laser configuration arises from two distinct mechanisms which have widely differing characteristics. Sisyphus cooling only occurs for blue detuning whilst VSCPT occurs whatever the detuning. We only consider here the case of blue detuning. The two mechanisms also have very different cooling times. Firstly, on a relatively short time scale, Sisyphus cooling takes place due to the spatially varying upper adiabatic potential, *i.e.*, motional coupling of the adiabatic potentials transfers a moving atom from the lower to the upper adiabatic potential preferentially at positions where the latter assumes a minimum. Subsequently the atom runs up the potential hill thereby transferring kinetic energy into potential energy which is finally removed from the system by a spontaneously emitted photon bringing the atom back into the flat lower potential.

Secondly, on a much longer time scale [7], VSCPT takes place, which causes the atomic population to accumulate in the dark state given by the wave function

$$|\psi_{\mathrm{D}}\rangle = \frac{1}{2}\Big[\mathrm{e}^{\mathrm{i}\theta/2}|-1;-\hbar k\rangle + \mathrm{e}^{-\mathrm{i}\theta/2}|-1;\hbar k\rangle + \mathrm{e}^{\mathrm{i}\theta/2}|1;\hbar k\rangle + \mathrm{e}^{-\mathrm{i}\theta/2}|1;-\hbar k\rangle\Big] \tag{6}$$

(in a ket $|m_F; p\rangle$ the first parameter refers to the Zeeman sublevel and the second to the atomic momentum along Oz). This state is completely decoupled from the laser light, and hence once an atom is in this state, it will remain there.

The momentum distribution associated with $|\psi_{\mathrm{D}}\rangle$ has two peaks located at $\pm\hbar k$. For $|\psi_{\mathrm{D}}\rangle$ these peaks are δ functions but in actual experiments they have a nonzero width which is used for measuring the temperature. An atom in the dark state is found at position z with a probability proportional to

$$P(z) = \sum_{m_F} |\langle m_F, z|\psi_{\mathrm{D}}\rangle|^2 = 1 + \cos\theta\cos(2kz). \tag{7}$$

This probability is maximum for $z = 0, \pm\lambda/2, \ldots$ and minimum for $z = \pm\lambda/4, \pm 3\lambda/4, \ldots$ (for $\theta \neq \pm\pi/2$).

2.2 Effect of neighbouring transitions

However, real atoms have a more complicated hyperfine structure and thus the laser light usually couples the $F = 1$ ground state to several excited states with angular momenta different from the favourable $F' = 1$. This disturbs the cooling on the $1 \rightarrow 1$ transition, and a completely dark state no longer exists. Of course, this effect depends strongly on the energy spacing of the excited state sublevels.

In the experiment we worked on the D_2 line of ^{87}Rb, where the most important disturbance of the lattice on the $1 \rightarrow 1$ transition comes from the close $F' = 0$ excited state (the energy separation between the $F' = 0$ and the $F' = 1$ excited state being $12.3\hbar\Gamma$, where Γ is the natural line width of the $5P_{3/2}$ level, $\Gamma = 2\pi \times 5.889\,\mathrm{MHz}$, see Fig. 1). Treating this off-resonant coupling of the lattice lasers to the $F' = 0$ state as a weak perturbation, one obtains in first order the lowest adiabatic potential

$$V'_{\mathrm{NC}}(z) = \frac{4}{3}U'_0\frac{\cos^2(kz + \theta/2)\cos^2(kz - \theta/2)}{\cos^2(kz + \theta/2) + \cos^2(kz - \theta/2)} \tag{8}$$

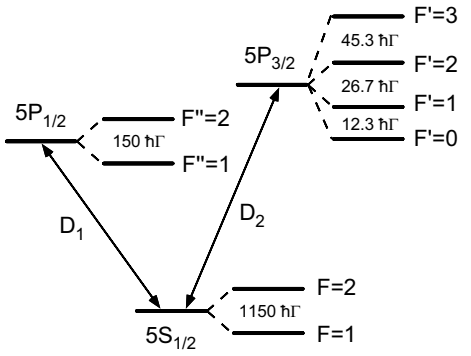

Fig. 1. Simplified level scheme of ^{87}Rb. Angular momenta of hyperfine levels are indicated, and the intervals between them given in terms of the natural line width of the $5P_{3/2}$ level, $\Gamma = 2\pi \times 5.889$ MHz.

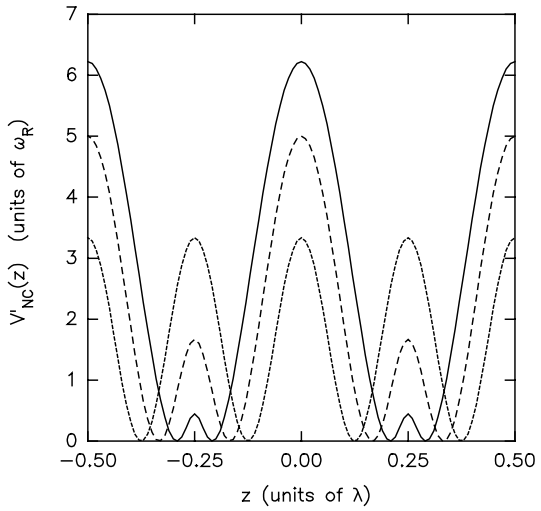

Fig. 2. Lowest adiabatic potential $V'_{\rm NC}(z)$ for $\theta = 30°$ (solid line), $\theta = 60°$ (long dashes), and $\theta = 90°$ (short dashes) for an optical potential depth $U'_0 = 10\omega_{\rm R}$.

instead of the flat potential $V_{\rm NC}(z)$ (Eq. (2)), where U'_0 denotes the light shift per beam on the $1 \rightarrow 0$ transition. Examples for this adiabatic potential for different lattice angles θ are plotted in Figure 2.

From the form of this potential we expect that the atoms will be localized around $z = \pm\lambda/4$ for small lattice angles, and around $z = \pm\lambda/8$, $\pm 3\lambda/8$ for $\theta = 90°$ ("lin $\perp$ lin" configuration) [12]. But for all values of θ the perturbed potential $V'_{\rm NC}(z)$ has maxima at $z = 0$, $\pm\lambda/2$, where the velocity-selective dark state of the pure $1 \rightarrow 1$ transition is localized, see equation (7). Hence, the coupling of the laser light to the neighbouring $F' = 0$ excited state efficiently destroys the velocity-selective dark state.

However, the combined system of the excited states $F' = 0$ and $F' = 1$ still exhibits *local* dark states at positions where the laser light is circularly polarized, *i.e.*, for $kz = \pm\theta/2 \pm \pi/2$. But even this local dark state is destroyed by taking the next neighbouring level $F' = 2$ into account (the energy spacing between the $F' = 1$ and $F' = 2$ state being $26.7\hbar\Gamma$).

Now the question arises for which parameters, such as hyperfine splitting, laser intensity, etc., the coupling to the neighbouring atomic states prevents the existence of VSCPT. We may estimate this threshold from the following considerations.

Although the lifetime of the exact VSCPT dark state is infinite, the time to reach this steady-state is also infinite. In any experiment, one thus obtains a momentum distribution which is peaked at the momenta $\pm\hbar k$, but still has a nonzero width. Atoms in these quasi-dark states are weakly coupled by motional coupling to the bright states, which, depending on their velocity, gives them a finite decay rate [3] of

$$\Gamma_{\rm NC}(p) \approx \Gamma \left(\frac{kp}{m}\right)^2 / \Omega^2, \tag{9}$$

where Ω is the Rabi frequency of a single laser beam. If we assume a width of the momentum distribution of $\hbar k/2$, the average decay rate of the quasi-dark states is given by

$$\overline{\Gamma_{\rm NC}} \approx \Gamma \omega_{\rm R}^2 / \Omega^2, \tag{10}$$

where $\omega_{\rm R} = \hbar k^2/(2m)$ is the recoil frequency. VSCPT will thus be destroyed if the optical pumping rate on the $1 \rightarrow 0$ transition, $\Gamma_{10} = \Gamma\Omega^2/\Delta_1^2$, is of the order of or larger than this mean decay rate, *i.e.*, for

$$\Gamma\Omega^2/\Delta_1^2 > \Gamma\omega_{\rm R}^2/\Omega^2, \tag{11}$$

where Δ_1 is the hyperfine splitting between the excited state sublevels $F' = 0$ and $F' = 1$. Because $U'_0 \sim \Omega^2/\Delta_1$, equation (11) is equivalent to

$$U'_0 > \omega_{\rm R}. \tag{12}$$

Thus, to obtain VSCPT one either has to work with atoms with a large hyperfine splitting, such as metastable helium [3], or one has to operate at very low laser intensity.

In our experiment the detuning $\Delta = \omega - \omega_0$ from the $1 \rightarrow 1$ transition was typically of the order of Γ. We had thus $U'_0/U_0 \sim \Gamma/\Delta_1$ and equation (12) reads $U_0 > \omega_{\rm R}\Delta_1/\Gamma$. Because $\Delta_1/\Gamma \sim 10$ we find that VSCPT could only be efficient in a domain well below the "decrochage" (low-intensity breakdown) of the Sisyphus effect. In fact, under practical experimental conditions equation (12) was fulfilled and we focused on the investigation of the Sisyphus cooling in a nearly dark lattice.

We may quantify the term "nearly dark" by comparing the scattering rate due to the $1 \rightarrow 0$ transition, Γ_{10}, with that in the quasi-dark state, $\overline{\Gamma_{\rm NC}}$. From the above arguments we find $\Gamma_{10}/\overline{\Gamma_{\rm NC}} \approx {U'_0}^2/\omega_{\rm R}^2$ and taking $U_0 \approx 100\omega_{\rm R}$ (corresponding to an intensity close to the decrochage in our experiments) yields $\Gamma_{10}/\overline{\Gamma_{\rm NC}} \approx 100$. On the other hand, the scattering rate in the corresponding bright lattice would be of the order of $\Gamma\Omega^2/\Delta^2 \approx 100\Gamma_{10}$.

3 Experimental setup

The experiment takes place in an evacuated quartz cell containing rubidium vapour at a pressure of $\sim 10^{-8}$ torr.

Two master diode lasers (one external cavity, one internal cavity) are locked to hyperfine transitions in the D_2 line of ^{87}Rb, and each master laser is used to injection-lock two slave diode lasers to provide light for trapping and repumping, and for the lattice and the lattice repumper.

Approximately 10^7 atoms of ^{87}Rb are first trapped and cooled to a temperature of about 25 μK in a magneto-optical trap operating at a detuning of -3Γ from the $F = 2 \rightarrow F' = 3$ hyperfine transition (repumping light resonant with the $1 \rightarrow 2$ transition is superimposed on the six trapping beams). The axial field gradient at the trap centre is approximately 7 G/cm.

After a trap loading period of 1 s, the magnetic field gradient is switched off (in $\lesssim 1$ ms) and the atoms undergo 8 ms of molasses cooling during which the intensity of the $2 \rightarrow 3$ beams is reduced in a series of steps. Next the molasses beams are turned off completely, first by fast ($\lesssim 10$ ns) extinction of the r.f. supply to an acousto-optic modulator (AOM) in the beam, then any residual light is blocked by a mechanical shutter; the same shutter cuts the repumping light.

Within 1 ms, the vertical counter-propagating lattice beams and associated repumping beams are switched on. The lattice beams are blue-detuned by a variable frequency Δ from the $1 \rightarrow 1$ transition; the detuning and intensity of these beams is controlled by AOMs, and they are switched by a combination of AOM and shutter as for the molasses beams; the angle between the linear polarizations of the two beams is controlled by a $\lambda/2$ waveplate. The lattice repumping light consists of two pairs of counter-propagating beams lying in the horizontal plane, one pair lying approximately at right angles to the other; it is blue-detuned by Γ from the $2 \rightarrow 2$ transition and is switched by a mechanical shutter.

The remainder of the experimental sequence depends on whether temperature measurements (Sect. 5) or probe absorption measurements (Sect. 6) are being made. Temperature is measured by a ballistic (time-of-flight) method. After approximately 6 ms the lattice repumping beams and the lattice beams are switched off (in that order to leave the atoms in the $F = 2$ ground state). The atoms fall freely and pass through a laser beam in the form of a thin horizontal sheet of light about 8 cm below the trap position, resonant with the $2 \rightarrow 3$ transition. The absorption of this beam as the atoms traverse it yields their velocity distribution; their initial temperature is obtained from the width of this distribution by fitting a Gaussian curve and correcting for geometrical factors due to the initial size of the trapped cloud of atoms and the thickness of the detection beam.

For probe absorption measurements, a weak probe beam is switched on with the lattice beams. This probe beam, resonant with the $1 \rightarrow 1$ transition, propagates at a small angle to the lattice beams ($1.2^\circ \pm 0.1^\circ$), has a much smaller area than they do (0.90 mm^2 compared with 28 mm^2), and is much less intense (the probe intensity was maintained at 0.5% of the intensity per lattice beam I, a value found to be sufficiently small that there was negligible effect on the temperature of the atoms in the lattice). The probe is linearly polarized with the polarization vector either parallel or perpendicular to the lattice axis (Fig. 3). The absorption of the probe beam by the lattice is obtained by measuring the transmission during and after the lattice (the signal being averaged over approximately 1 ms in each case), which must be done every experimental sequence because of variations in scattered light levels. Undesired absorption of the probe after the end of the lattice period is eliminated by extinguishing the lattice light after its repumping light, thus ensuring all atoms are optically pumped out of the $F = 1$ lower level before the probe transmission is measured. The geometry of the lattice, lattice repumper and probe beams is illustrated in Figure 3.

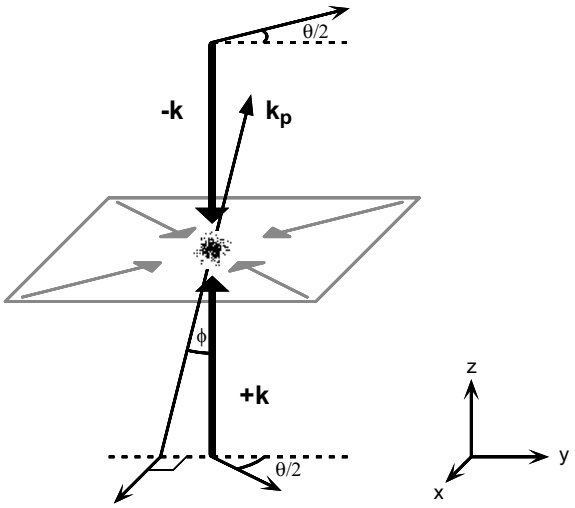

Fig. 3. Geometry of lattice, lattice repumper and probe beams in the experiment. The counter-propagating lattice beams $\pm\mathbf{k}$ have an angle θ between their linear polarizations. The probe beam $\mathbf{k}_\mathrm{p}$ makes a slight angle ϕ with the lattice beams, exaggerated here for clarity (in fact $\phi = 1.2^\circ \pm 0.1^\circ$); it is shown here with its polarization perpendicular to the lattice axis (dotted lines). The lattice repumping beams, propagating in the xy-plane, are also indicated.

Whether for temperature or probe absorption measurements, the experimental sequence must be repeated many times to obtain an acceptable signal-to-noise ratio; typically signals are averaged over 20 sequences. Other important experimental considerations are compensation of stray magnetic fields and elimination of scattered light, *e.g.* from the trapping laser; both these factors reduce the cooling efficiency of the nearly dark lattice. Stray magnetic fields are cancelled by three orthogonal compensation coils and we adjust the DC current in each of these iteratively to minimize the temperature of the atoms in the lattice. In this manner DC magnetic fields are compensated to $\lesssim 10$ mG; the amplitudes of residual AC magnetic fields were measured to be of the same order of magnitude.

Scattered light is blocked by the mechanical shutters described previously and by shielding the interaction region from the rest of the optics. These precautions allowed us to achieve temperatures in the 1D lattice as low as 3 μK.

4 Theoretical approach: Quantum Monte-Carlo simulations

We will compare our experimental results with numerically obtained solutions of the atomic master equation which describes the dynamics of the atomic density operator ρ restricted to the ground state manifold by adiabatic elimination of the excited states. This master equation is given by

$$\dot{\rho} = -\mathrm{i}\left[h_{\mathrm{eff}}\rho - \rho h_{\mathrm{eff}}^{\dagger}\right] + \sum_{F'=0,1,2}\gamma_{F'}\sum_{\sigma=0,\pm1}\int_{-k}^{k}\frac{\mathrm{d}u}{k}N_{\sigma}\left(\frac{u}{k}\right) \times\left[\mathrm{e}^{-\mathrm{i}u\hat{x}}\hat{B}_{\sigma}^{F'}\right]\rho\left[\hat{B}_{\sigma}^{F'\dagger}\mathrm{e}^{\mathrm{i}u\hat{x}}\right] \quad (13)$$

where the effective Hamiltonian h_{eff},

$$h_{\mathrm{eff}} = \frac{\hat{p}^2}{2m} + \sum_{F'=0,1,2}\left(U_{F'} - \frac{\mathrm{i}}{2}\gamma_{F'}\right)\sum_{\sigma=0,\pm1}\hat{B}_{\sigma}^{F'\dagger}\hat{B}_{\sigma}^{F'}, \quad (14)$$

describes the coherent interaction of the atom with the light field and the decay of the atomic ground states due to optical pumping, and the second term in equation (13) gives rise to the changes of the atomic state according to optical pumping. In equations (13, 14) the operators $\hat{B}_{\sigma}^{F'}$ describe Raman transitions consisting of the absorption of a single laser photon (which excites the atom to the F' excited state) and the subsequent spontaneous emission of a σ-polarized photon, $U_{F'}$ ($\gamma_{F'}$) is the optical potential depth (optical pumping rate) of a single laser beam on the $1 \rightarrow F'$ transition, and $N_{\sigma}(q)$ is the angular distribution of spontaneously emitted photons. For a derivation and a more detailed description of this master equation see, *e.g.*, reference [13].

We numerically solve equation (13) for the atomic steady state by a fully quantum wavefunction Monte-Carlo simulation technique [7,14,15]. The basic idea of this method is to integrate the time evolution of the atomic wavefunction governed by the effective Hamiltonian h_{eff}, and to apply quantum jumps described by the operators $\hat{B}_{\sigma}^{F'}$ to this wavefunction at random times but with the appropriate distribution. By averaging over many simulations of this kind one obtains the steady-state density operator and thus one can calculate all required quantities, such as temperatures, momentum and spatial distributions, atomic polarizations etc.

5 Results: Temperature measurements

Experimental measurements of the temperature T were performed as described in Section 3. We studied the variation of T with I (intensity per lattice beam), Δ (frequency detuning), and θ (angle between the lattice beam polarizations). The axes in the figures are labelled with the experimental parameters (T in μK, I in mW/cm^2, etc.). The conversion to other useful units ($T_{\mathrm{R}} = (\hbar k)^2/(mk_{\mathrm{B}})$, U_0/ω_{R}, etc.) is given in the figure captions (for example, $T_{\mathrm{R}} = 0.36$ μK in rubidium). Note, however, that the data depend on the values of atomic parameters and that the calculations were performed for the case of the D_2 transitions of ^{87}Rb.

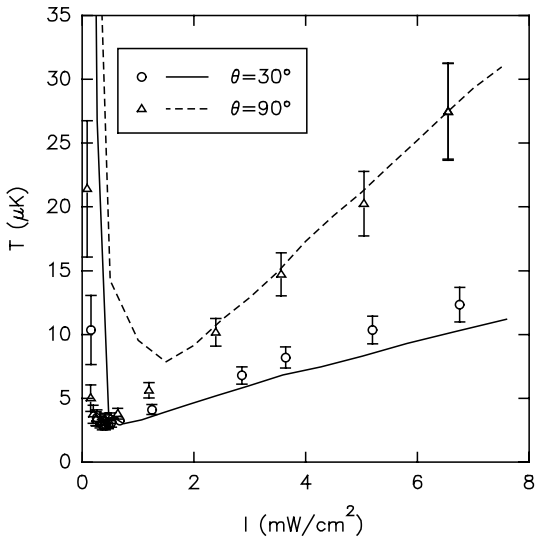

Fig. 4. Temperature *vs.* lattice intensity for $\theta = 30°$ and $\theta = 90°$. The experiments were performed at a detuning $\Delta = 2\Gamma$. The intensity $I = 1$ mW/cm^2 corresponds to a light shift $U_0 = 97\omega_{\mathrm{R}}$, the recoil temperature $T_{\mathrm{R}} = (\hbar k)^2/(mk_{\mathrm{B}})$ is equal to 0.36 μK for Rb. The curves correspond to the predictions of the Monte-Carlo simulations.

We show in Figure 4 the variation of T *versus* I for $\theta = 30°$ and $\theta = 90°$, for a detuning of $\Delta = 2\Gamma$. The general dependence, *i.e.*, linear variation at high intensity and decrochage at low intensity, corresponds to what is expected from Sisyphus cooling. The fact that Sisyphus cooling occurs for $\theta = 90°$ further demonstrates the importance of the $F' = 0$ and $F' = 2$ levels because Sisyphus cooling is not predicted for a pure $F = 1 \rightarrow F' = 1$ transition in the lin $\perp$ lin configuration [6].

One also notices that the lowest temperature $T_{\mathrm{min}} \simeq 3$ μK remains significantly larger than T_{R} ($T_{\mathrm{min}} \simeq 8.3T_{\mathrm{R}}$). This shows that we do not reach the regime of VSCPT on this transition. The curves in Figure 4 correspond to the predictions of the quantum Monte-Carlo simulations; we remark that there are no adjustable parameters in these calculations. The agreement with the experimental results is excellent at high intensities above the decrochage. At low intensity the experimental values are lower than the theoretical ones. This is probably because fast atoms are lost in the experiment below the decrochage and there is thus a selection of ultra cold atoms.

We present in Figure 5 the variation of T with θ for fixed $\Delta = 2\Gamma$ and fixed I ($I = 2.1$ mW/cm^2 and $I = 6.8$ mW/cm^2). As expected the temperature exhibits two peaks, a very large one at $\theta = 0°$ where there is absolutely no polarization gradient cooling, and a smaller one at $\theta = 90°$ where the polarization gradient cooling

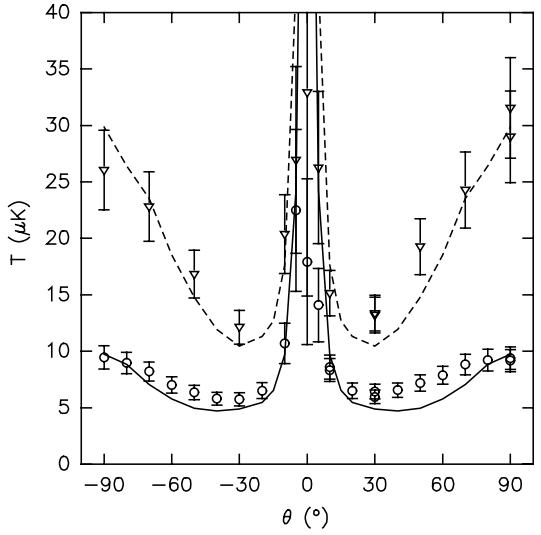

Fig. 5. Temperature *vs.* lattice angle for detuning $\Delta = 2\Gamma$ and lattice intensity $I = 2.1$ mW/cm^2 (circles and solid curve) and $I = 6.8$ mW/cm^2 (triangles, dashed curve). These two intensities respectively correspond to $U_0 = 200\omega_{\rm R}$ and $U_0 = 660\omega_{\rm R}$.

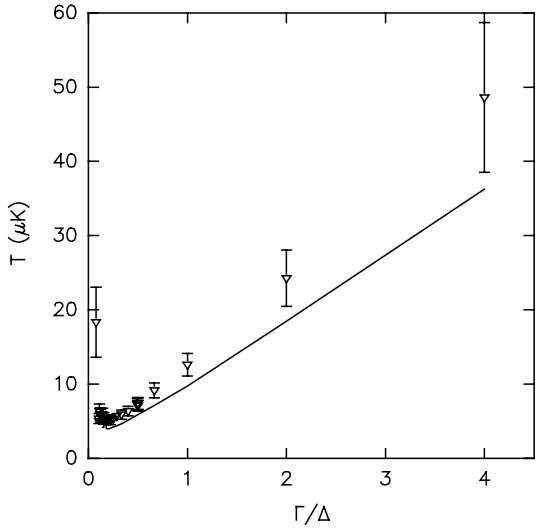

Fig. 6. Temperature *vs.* inverse of detuning for lattice intensity $I = 2.1$ mW/cm^2 and $\theta = 60°$. $\Gamma/\Delta = 1$ corresponds to $U_0 = 345\omega_{\rm R}$.

originates *only* from the distant $F' = 0$ and $F' = 2$ sublevels. The minimum of the temperature is found near $\theta = 30°$.

The experimental values are compared with the results of the quantum Monte-Carlo simulations. An excellent agreement is found apart from a few points near $\theta = 0°$ where the experimental value is lower than the theoretical one. This difference is probably due to impure polarization of the lattice beams.

Finally, we present in Figure 6 the variation of T *versus* Γ/Δ for $I = 2.1$ mW/cm^2 and $\theta = 60°$. Here also the variation of T corresponds to what is expected for Sisyphus cooling, *i.e.*, a linear variation for large values of Γ/Δ and a decrochage when $\Gamma/\Delta \to 0$. The experimental measurements are in satisfactory agreement with the quantum Monte-Carlo simulations. If we compare these data with those obtained by changing the intensity, we find an asymptotic behaviour of $T = (I/\Delta)5.7$ μK (where I is in units of mW/cm^2 and Δ in units of Γ) here, whereas a value of $T = (I/\Delta)6.6$ μK was found by varying I. Thus, apart from a 15% difference in these values, there is a reasonably good agreement with the qualitative behaviour of Sisyphus cooling in bright lattices.

6 Results: Probe absorption

Let us now consider a supplementary probe beam with electric field

$$\mathbf{E}_{\rm p} = \boldsymbol{\mathcal{E}}_{\rm p} \cos(\mathbf{k}_{\rm p} \cdot \mathbf{r} - \omega_{\rm p} t) \tag{15}$$

of very weak intensity that interacts with the atoms (in the experiment this intensity is approximately 0.5% of the lattice intensity).

We will first evaluate the probe absorption in the case of pure dark state cooling. We thus assume that the unperturbed state of the system is $|\psi_{\rm D}\rangle$ (6), calculate the state $|\tilde{\psi}\rangle$ in the presence of the probe beam using first-order perturbation theory and find the dipole moment $\langle \mathbf{d} \rangle = \langle \tilde{\psi} | \mathbf{d} | \tilde{\psi} \rangle$. If we denote by $\mathbf{e}_y$ the unit vector for the bisectrix of the lattice polarizations and $\mathbf{e}_x$ the unit vector for the orthogonal direction (Fig. 3), we look for a variation of the form

$$\langle d_x \rangle = \frac{\mathcal{E}_0}{2} \left[\alpha_x (\boldsymbol{\mathcal{E}}_{\rm p} \cdot \mathbf{e}_x) + \alpha_{xy} (\boldsymbol{\mathcal{E}}_{\rm p} \cdot \mathbf{e}_y) \right] \times \mathrm{e}^{\mathrm{i}(\mathbf{k}_{\rm p} \cdot \mathbf{r} - \omega_{\rm p} t)} + c.c., \tag{16}$$

$$\langle d_y \rangle = \frac{\mathcal{E}_0}{2} \left[\alpha_{yx} (\boldsymbol{\mathcal{E}}_{\rm p} \cdot \mathbf{e}_x) + \alpha_y (\boldsymbol{\mathcal{E}}_{\rm p} \cdot \mathbf{e}_y) \right] \times \mathrm{e}^{\mathrm{i}(\mathbf{k}_{\rm p} \cdot \mathbf{r} - \omega_{\rm p} t)} + c.c. \tag{17}$$

In fact, denoting $\Delta_{\rm p} = \omega_{\rm p} - \omega_0$, the direct calculation gives

$$\langle d_x \rangle = \frac{-d^2 \mathrm{e}^{\mathrm{i}(\mathbf{k}_{\rm p} \cdot \mathbf{r} - \omega_{\rm p} t)}}{16\hbar(\Delta_{\rm p} + \mathrm{i}\Gamma/2)} \times \Big\{ \left[\cos(kz + \theta/2) + \cos(kz - \theta/2) \right]^2 (\boldsymbol{\mathcal{E}}_{\rm p} \cdot \mathbf{e}_x) + \mathrm{i} \left[\cos^2(kz + \theta/2) - \cos^2(kz - \theta/2) \right] (\boldsymbol{\mathcal{E}}_{\rm p} \cdot \mathbf{e}_y) \Big\} + c.c. \tag{18}$$

However, we only need the spatial average value of the term inside the bracket. Hence we find

$$\alpha_x = -\frac{d^2}{8\mathcal{E}_0 \hbar(\Delta_{\rm p} + \mathrm{i}\Gamma/2)} (1 + \cos\theta), \tag{19}$$

$$\alpha_{xy} = 0, \tag{20}$$

and similarly

$$\alpha_y = -\frac{d^2}{8\mathcal{E}_0 \hbar(\Delta_{\rm p} + \mathrm{i}\Gamma/2)} (1 - \cos\theta), \tag{21}$$

$$\alpha_{yx} = 0. \tag{22}$$

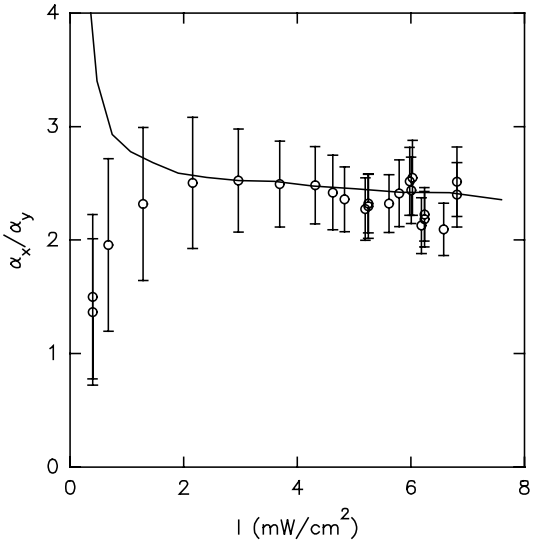

Fig. 7. Ratio α_x/α_y of the absorption coefficients for probe polarizations orthogonal (α_x) and parallel (α_y) to the lattice axis, as a function of lattice intensity I. The lattice detuning is $\Delta = 2\Gamma$ and the polarization angle is $\theta = 30°$.

As expected from the symmetry of the problem, the axes $\mathbf{e}_x$ and $\mathbf{e}_y$ are the axes under which the light polarization does not change. The ratio of the absorption coefficients along $\mathbf{e}_x$ and $\mathbf{e}_y$ is

$$\frac{\alpha_x}{\alpha_y} = \frac{1+\cos\theta}{1-\cos\theta}\,. \tag{23}$$

This result is associated with the localization of the dark state (6) which is maximum for $z = 0, \pm\lambda/2, \ldots$, *i.e.*, at points where the lattice field polarization is $\mathbf{e}_y$. As a result, an x-polarized probe beam will experience a stronger absorption than a y-polarized probe beam.

How do we expect these results to be modified for the ^{87}Rb transition? Because $\mathbf{e}_x$ and $\mathbf{e}_y$ remain the axes of symmetry of the problem, we still expect them to be the neutral axes of the birefringent medium. By contrast, we noticed that the localization in ^{87}Rb differs from that of the dark state. We thus expect to find a reduced value for α_x/α_y.

All these results are well confirmed both by the experiment and by the quantum Monte-Carlo simulation. We show in Figure 7 the variation of α_x/α_y *versus* I for $\Delta = 2\Gamma$ and $\theta = 30°$. The circles correspond to the experiment and the line to the simulation. The asymptotic value of α_x/α_y is equal to 2.4 whilst a value of 13.9 is predicted from equation (23) for a pure dark state. The agreement between the experiment and the simulation is very good apart from a few points at low intensity. A possible reason for the disagreement at low intensity is that the atoms have not attained an equilibrium state in the experiment.

7 Conclusions

In conclusion, we have presented the results of an investigation of the cooling and trapping of atoms near an $F = 1 \rightarrow F' = 1$ transition in rubidium. The experimental results are generally in excellent agreement with the theoretical predictions; we emphasize that the theoretical results are *ab initio* calculations with no free parameters. This study shows the difficulty of achieving VSCPT in many real atoms because of the inhibiting effect of neighbouring transitions. VSCPT can only be achieved on a very well isolated transition.

This work was supported by the European Commission TMR Network on Quantum Structures (contract number FMRX-CT96-0077). We are very grateful to Cécile Robilliard and Luca Guidoni for helpful discussions.

References

1. J. Dalibard, C. Cohen-Tannoudji, J. Opt. Soc. Am. B **6**, 2023 (1989).
2. P.J. Ungar, D.S. Weiss, E. Riis, S. Chu, J. Opt. Soc. Am. B **6**, 2058 (1989).
3. A. Aspect, E. Arimondo, R. Kaiser, N. Vansteenkiste, C. Cohen-Tannoudji, Phys. Rev. Lett. **61**, 826 (1988).
4. P.S. Jessen, C. Gerz, P.D. Lett, W.D. Phillips, S.L. Rolston, R.J.C. Spreeuw, C.I. Westbrook, Phys. Rev. Lett. **69**, 49 (1992); M. Gatzke, G. Birkl, P.S. Jessen, A. Kastberg, S.L. Rolston, W.D. Phillips, Phys. Rev. A **55**, R3987 (1997).
5. T. Lawall, S. Kulin, B. Saubamea, N. Bigelow, M. Leduc, C. Cohen-Tannoudji, Phys. Rev. Lett. **75**, 4194 (1995).
6. M.S. Shahriar, P.R. Hemmer, M.G. Prentiss, P. Marte, J. Mervis, D.P. Katz, N.P. Bigelow, T. Cai, Phys. Rev. A **48**, R4035 (1993).
7. P. Marte, R. Dum, R. Taïeb, P. Zoller, M.S. Shahriar, M. Prentiss, Phys. Rev. A **49**, 4826 (1994).
8. M. Weidemüller, T. Esslinger, M. Olshanii, A. Hemmerich, T. Hänsch, Europhys. Lett. **27**, 109 (1994).
9. M. Widmer, M.J. Bellanca, W. Buell, H. Metcalf, M. Doery, E. Vredenbregt, Optics Lett. **21**, 606 (1996).
10. T. Esslinger, F. Sander, M. Weidemüller, A. Hemmerich, T.W. Hänsch, Phys. Rev. Lett. **76**, 2432 (1996).
11. J. Guo, P.R. Berman, Phys. Rev. A **48**, 3225 (1993).
12. H. Stecher, H. Ritsch, P. Zoller, F. Sander, T. Esslinger, T.W. Hänsch, Phys. Rev. A **55**, 545 (1997); D. Boiron, C. Triché, D.R. Meacher, P. Verkerk, G. Grynberg, Phys. Rev. A **52**, R3425 (1995).
13. C. Menotti, P. Horak, H. Ritsch, J.H. Müller, E. Arimondo, Phys. Rev. A **56**, 2123 (1997).
14. J. Dalibard, Y. Castin, K. Mølmer, Phys. Rev. Lett. **68**, 580 (1992); K. Mølmer, Y. Castin, J. Dalibard, J. Opt. Soc. Am. B **10**, 524 (1993).
15. R. Dum, P. Zoller, H. Ritsch, Phys. Rev. A **45**, 4879 (1992).